

Functional Mechanisms Shaping Lateral Geniculate Responses to Artificial and Natural Stimuli

Valerio Mante,^{1,*} Vincent Bonin,¹ and Matteo Carandini¹

¹The Smith-Kettlewell Eye Research Institute, 2318 Fillmore Street, San Francisco, CA 94115, USA

*Correspondence: valerio@monkeybiz.stanford.edu

DOI 10.1016/j.neuron.2008.03.011

SUMMARY

Functional models of the early visual system should predict responses not only to simple artificial stimuli but also to sequences of complex natural scenes. An ideal testbed for such models is the lateral geniculate nucleus (LGN). Mechanisms shaping LGN responses include the linear receptive field and two fast adaptation processes, sensitive to luminance and contrast. We propose a compact functional model for these mechanisms that operates on sequences of arbitrary images. With the same parameters that fit the firing rate responses to simple stimuli, it predicts the bulk of the firing rate responses to complex stimuli, including natural scenes. Further improvements could result by adding a spiking mechanism, possibly one capable of bursts, but not by adding mechanisms of slow adaptation. We conclude that up to the LGN the responses to natural scenes can be largely explained through insights gained with simple artificial stimuli.

INTRODUCTION

A central goal of visual neuroscience is to understand the processing performed by the early visual system on the flow of complex images that stimulate the eyes. Virtually all progress toward this goal has come from studies that used simple stimuli such as dots, bars, and gratings. Such simple, artificial stimuli present overwhelming advantages in terms of experimental control: their simple visual features can be tailored to isolate one or few of the several mechanisms shaping the responses of visual neurons (Rust and Movshon, 2005). Ultimately, however, we need to understand how neurons respond not only to these simple stimuli but also to image sequences that are arbitrarily complex, including those encountered in natural vision. The visual system evolved while viewing complex scenes, and its function may be uniquely adapted to the structure of natural images (Felsen and Dan, 2005; Simoncelli and Olshausen, 2001). In fact, it has been suggested that artificial and natural stimuli may engage entirely different mechanisms (Felsen and Dan, 2005; Olshausen and Field, 2005).

The chasm between the knowledge gained with artificial stimuli and the world of natural stimuli can be gauged in the lateral geniculate nucleus (LGN). The LGN constitutes a testbed for

theories of visual function: its responses are complex enough to constitute a challenge, but enough understood to make a general model appear within reach. Such a functional model would be useful, as it would summarize much of the processing performed in the retina, and it would characterize the main visual input to the cerebral cortex. Can such a general functional model of LGN responses be derived based on present knowledge? Would the model predict responses to both simple, artificial stimuli and complex, natural scenes?

Decades of research in retina and LGN have yielded detailed models of the mechanisms shaping responses to simple, artificial stimuli (Carandini et al., 2005; Kaplan and Benardete, 2001; Meister and Berry, 1999; Shapley and Enroth-Cugell, 1984; Troy and Shou, 2002; Victor, 1999). At a minimum, these mechanisms include a center-surround linear receptive field (RF) followed by a nonlinearity that produces firing rates (Figure 1A) (Cai et al., 1997; Dan et al., 1996; Dawis et al., 1984; Saul and Humphrey, 1990; So and Shapley, 1981; Stanley et al., 1999). The RF, in turn, depends on local statistics of the images through the fast adaptation mechanisms of light adaptation and contrast gain control (Figure 1B) (Bonin et al., 2005; Demb, 2002; Kaplan and Benardete, 2001; Lesica et al., 2007; Mante et al., 2005; Meister and Berry, 1999; Shapley and Enroth-Cugell, 1984). The former operates largely in the retina (Fain et al., 2001; Meister and Berry, 1999; Shapley and Enroth-Cugell, 1984); the latter begins in the retina (Baccus and Meister, 2002; Demb, 2002; Meister and Berry, 1999; Shapley and Enroth-Cugell, 1984; Shapley and Victor, 1978; Victor, 1987) and becomes progressively stronger at later stages in the visual pathway (Sclar et al., 1990). Moreover, additional mechanisms may play an important role, including slow contrast adaptation (Baccus and Meister, 2002; Demb, 2002; Solomon et al., 2004), single spike generation (Butts et al., 2007; Carandini et al., 2007; Keat et al., 2001; Pillow et al., 2005), and burst generation (Lesica and Stanley, 2004; Sherman, 2001).

Most of these models, however, apply only to a restricted set of simple stimuli and do not generalize to more complex stimuli. Most of the difficulties are encountered with models of fast adaptation mechanisms. Unlike mechanisms of spike generation and burst generation, these mechanisms need to operate on sequences of images and must therefore be specified in the domains of both space and time. Models of light adaptation are generally limited to spatially uniform stimuli (e.g., van Hateren et al., 2002 and references therein) or full field gratings (Mante et al., 2005; Purpura et al., 1990); those models that operate both in space and in time do not account for contrast gain control (Dahari and Spitzer, 1996; Gaudiano, 1994; van Hateren, 2007). Similarly, models of contrast gain control operate in the domain either of

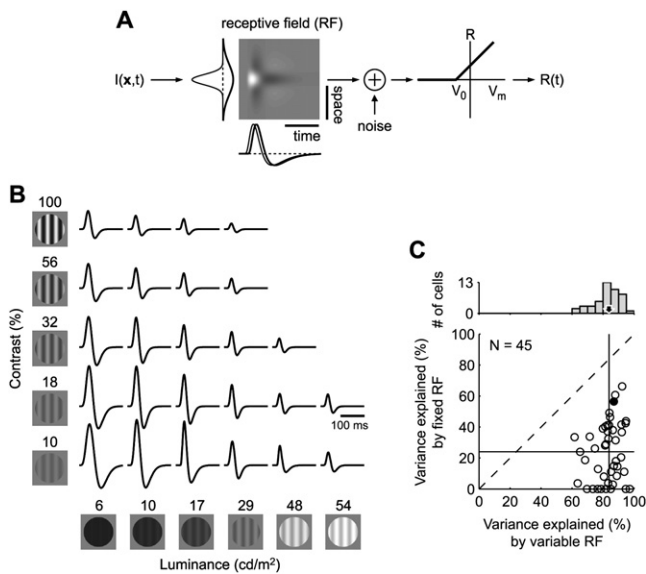


Figure 1. The Effects of Fast Adaptation on the Receptive Field

(A) The receptive field (RF) consists of a center filter (thin line) and an antagonistic, delayed surround (thick). Both center and surround have a Gaussian spatial profile (left) and a biphasic temporal weighting function (bottom). Fast adaptation operates by adjusting the temporal weighting function to the luminance and contrast of the stimulus. Firing rates (R) are obtained by convolving the RF with the stimulus, adding Gaussian noise, and rectifying the resulting membrane potential (V_m).

(B) The weighting function of the example neuron estimated at various combinations of luminance and contrast. Stimuli in the empty corner of the matrix are not physically realizable.

(C) The fraction of stimulus-driven variance in the responses explained by the full matrix (B) of weighting functions (horizontal axis) compared to fraction explained by a fixed weighting function estimated at intermediate luminance and contrast (vertical axis). The example neuron is in black. Filled lines and arrow indicate the medians of the distributions.

space (Bonin et al., 2005) or of time (Mante et al., 2005; van Hateren et al., 2002; Victor, 1987), but not in both domains. As a result, it is difficult to quantitatively relate studies employing complex, natural stimuli (Butts et al., 2007; Dan et al., 1996; Denning and Reinagel, 2005; Lesica et al., 2007; Lesica and Stanley, 2004; Stanley et al., 1999) to much of the literature on fast adaptation.

We therefore sought a model of LGN responses that extends previous, partial models of LGN responses by integrating the basic mechanisms of RF and firing rate generation together with the fast adaptation mechanisms of light adaptation and contrast gain control. We validated and constrained the model with simple artificial stimuli and then applied it to complex stimuli, both artificial and natural. By looking at the successes of the model, we show how the mechanisms of fast adaptation are central in shaping LGN responses to complex, natural stimuli. By investigating the model's shortcomings, we then assess the importance of the key additional mechanisms that may play a role in determining these responses.

RESULTS

We recorded from LGN neurons in anesthetized cats, subjecting each neuron to a battery of initial basic measurements that char-

acterized its linear RF (Figure 1A). We recorded responses to drifting gratings varying in location, spatial frequency, and temporal frequency (Figure S1 available online). As expected from previous studies (Cai et al., 1997; Dawis et al., 1984; Saul and Humphrey, 1990; So and Shapley, 1981), the responses to these stimuli were well described by a center-surround linear spatio-temporal RF followed by a nonlinearity that produces firing rates, and allowed us to estimate the parameters of these mechanisms (Figure 1A).

The RF, however, is not a fixed attribute; its gain and temporal profile depend on mechanisms of light adaptation and contrast gain control (Figure 1B). Increases in luminance or contrast diminish both the amplitude of the RF, the neuron's gain, and the duration of its temporal profile, the neuron's integration time (Bonin et al., 2005; Demb, 2002; Kaplan and Benardete, 2001; Lesica et al., 2007; Mante et al., 2005; Meister and Berry, 1999; Shapley and Enroth-Cugell, 1984). We characterized these mechanisms by recording responses to drifting gratings with several combinations of luminance and contrast (Figure S2), each varying over the range found in typical natural scenes (Mante et al., 2005). We used these responses to obtain a temporal weighting function for each combination of luminance and contrast (Figure 1B). The size and shape of these weighting functions reflect the corresponding gain and temporal profile of the RF.

The effects of fast adaptation on the gain and integration time of the RF were pronounced for all neurons in our sample (Figure 1C). As a consequence, letting the RF vary as appropriate from one stimulus condition to another substantially improves the model's ability to predict the responses. For the example cell (Figure 1B), the fraction of stimulus-driven variance in the responses explained is 87% for a variable RF and 56% for a fixed RF. Similar results are seen across the population (Figure 1C), where a variable RF explains 84% of the stimulus-driven variance (median, $n = 45$) compared to only 24% for a fixed RF.

A Model of Fast Adaptation

To obtain a succinct model of fast adaptation, we took advantage of the fact that the effects of light adaptation and contrast gain control are functionally separable (Mante et al., 2005). We therefore considered a succession of three independent stages: a fixed linear filter (an immutable property of the LGN neuron) and two adaptive mechanisms that modify its output.

We modeled the adaptive mechanisms as resistor-capacitor (RC) circuits whose conductances are allowed to vary with the input (Figure 2A). RC circuits or similar components have long been used to model adaptive mechanisms in retina and cortex (Baylor et al., 1974; Benardete and Kaplan, 1999; Brodie et al., 1978; Carandini et al., 1997; Fuortes and Hodgkin, 1964; Purpura et al., 1990; Shapley and Enroth-Cugell, 1984; Shapley and Victor, 1981; Victor, 1987). Here, a first batch of RC circuits implements light adaptation, while a second batch of RC circuits implements contrast gain control. For simplicity, in text and illustrations we refer to each batch of RC circuits as to a single RC stage; a full explanation is in the Experimental Procedures.

Only two model parameters were allowed to vary across stimulus conditions. The conductance of the first RC stage (the one devoted to light adaptation) was allowed to vary with luminance

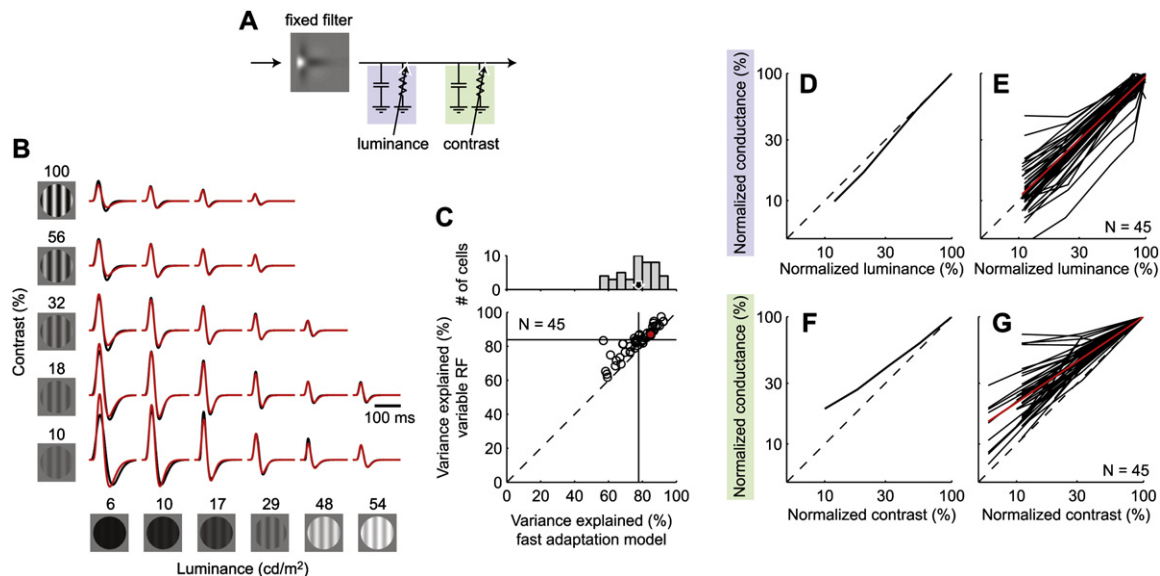


Figure 2. A Model of Fast Adaptation

(A) In the model, the effects of fast adaptation on the temporal weighting function are captured by two resistor-capacitor (RC) stages that shape the output of a fixed linear filter. The first RC stage implements light adaptation, and its conductance depends on stimulus luminance. The second RC stage implements contrast gain control, and its conductance depends on stimulus contrast. All other model parameters are fixed for a given neuron.

(B) Temporal weighting functions, measured (black, same as Figure 1B) and fitted by the model (red).

(C) The fraction of stimulus-driven variance in the response histograms explained by the fitted (horizontal axis) and measured (vertical axis) temporal weighting functions. Filled lines and arrow are medians of the distributions. The example neuron is drawn red.

(D) Dependence of first conductance on luminance, for example neuron.

(E) Same, for population (red line is linear regression over all neurons).

(F and G) Dependence of second conductance on contrast.

(Figures 2D and 2E), and that of the second RC stage (the one devoted to contrast gain control) was allowed to vary with contrast (Figures 2F and 2G). For fixed values of luminance and contrast (i.e., with fixed conductances), these stages act as linear filters, and thus the model reduces to a single RF. The temporal weighting function of this RF is the convolution of the weighting functions of the fixed linear filter and of the two RC stages (Mante et al., 2005).

This RC model captures the responses for the full range of luminance and contrast levels tested. It provides excellent fits to the estimated temporal weighting functions (Figure 2B, compare black and red). The model explains 85% of the stimulus-driven variance in the responses of the example cell and 78% (median, $n = 45$) over the entire population (Figure 2C, horizontal axis). Thus, with a dramatically reduced number of parameters, this model of fast adaptation fits the data practically as well as the full set (Figure 1B) of individually estimated RFs (Figure 2C, vertical axis).

The fits reveal a pleasingly simple relationship between model conductances and stimulus attributes, which can be used to compare the two adaptive mechanisms. The functions relating conductance to luminance (Figures 2D and 2E) and contrast (Figures 2F and 2G) are well approximated by power laws (straight lines in the logarithmic plots of Figures 2D–2G). The exponent of this power law is close to unity for light adaptation and markedly lower for contrast gain control (0.95 ± 0.05 versus 0.68 ± 0.05 , 95% confidence interval, $n = 45$, Figures 2E and 2G, red lines).

To interpret these results, consider that for stimuli of low temporal frequency the conductances of the RC stages are inversely proportional to the gain of responses (see *Experimental Procedures*). At low frequencies, therefore, light adaptation over this range of luminance levels is nearly perfect: it obeys Weber's law, i.e., a fractional increase in luminance results in the same fractional reduction in gain (Shapley and Enroth-Cugell, 1984). Contrast gain control, on the other hand, is weaker, as changes in contrast are not fully compensated by changes in gain.

The Spatial Footprint of Fast Adaptation

Before the model can be applied to arbitrary scenes, we must specify the spatial footprint of the light adaptation and contrast gain control stages, i.e., how the signals driving these mechanisms are integrated over visual space.

The footprint of light adaptation has been extensively studied in the retina. Light adaptation is thought to be driven by the average light intensity falling over a region not larger, and possibly smaller, than the RF surround (Cleland and Enroth-Cugell, 1968; Cleland and Freeman, 1988; Cohen et al., 1981; Enroth-Cugell et al., 1975; Enroth-Cugell and Shapley, 1973b; Lankheet et al., 1993b). For simplicity, we set the conductance of the light adaptation stage to the mean luminance falling on the RF surround. This choice guarantees that light adaptation operates locally and yet does not significantly deform the sinusoidal response to drifting gratings of optimal spatial and temporal frequency.

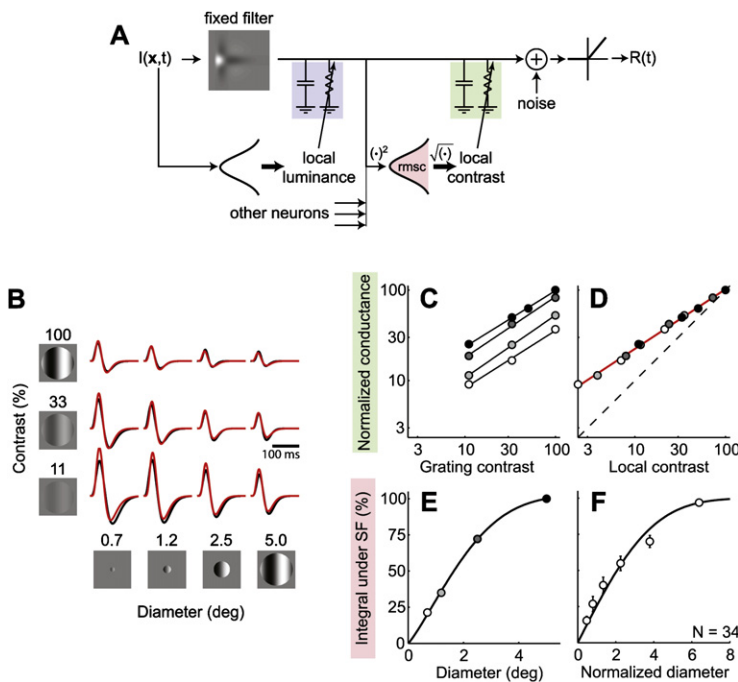


Figure 3. The Spatial Footprint of Fast Adaptation

(A) Local luminance is the average luminance falling over the RF in a recent period of time. Local contrast is computed by the suppressive field, by taking the square root of the squared and integrated responses of a pool of subunits.

(B) The temporal weighting function measured with gratings of various contrast and diameter (black). Fits of the model (red) were obtained by estimating one conductance value for the second RC stage for each combination of contrast and diameter.

(C) The estimated conductance increases with both contrast (abscissa) and diameter (white to black).

(D) The four sets of conductance values can be aligned by shifting them along the horizontal axis. The resulting curve describes how conductance depends on local contrast. Red line is linear regression.

(E) The volume under the portion of the suppressive field covered by the stimuli of different diameter. The data points are obtained from the magnitude of the shifts needed to align the curves in (C). The curve is the fit of a descriptive function (Experimental Procedures). For this neuron, the size of the center of the RF is 1.0°.

(F) Average over all neurons. Stimulus diameter is normalized by the size of the center of the RF. Error bars indicate two SE.

Similarly, contrast gain control depends on the root-mean-square contrast falling over a region centered over the RF (Shapley and Victor, 1979, 1981), which we term suppressive field (Bonin et al., 2005, 2006). We posit that this measure of local contrast sets the conductance of the contrast gain control RC stage (Figure 3A).

The validity of this choice can be tested on the basis of a simple prediction: increasing the size of a grating should affect the gain and the integration time of the RF exactly in the same way as a matched increase in contrast (Shapley and Victor, 1979, 1981). Indeed, in the model both manipulations result in stronger effects of contrast gain control. We confirmed this prediction by measuring temporal weighting functions from responses to drifting gratings varying in contrast and diameter. Indeed, increasing diameter reduced both the gain and the integration time, the same effects seen when increasing contrast (Figure 3B, black). To model these effects, we allowed the conductance of the contrast gain control stage (Figure 3A) to vary with stimulus diameter as well as contrast (Figure 3C). The resulting temporal weighting functions closely resemble the ones estimated individually (Figure 3B, compare black and red) and predict the responses to gratings of various contrast and diameter almost as well (72% versus 75% stimulus-driven variance explained for the example cell; 77% versus 82% over the population, $n = 34$, median). The curves relating grating contrast to conductance, which depend on grating diameter (Figure 3C), could be made to lie on a single line by appropriate horizontal shifts (Figure 3D) indicating that the effects of increasing diameter could be exactly matched by an appropriate increase in contrast. The horizontal shifts determine the weight contributed by each stimulus diameter (Figures 3E and 3F), and therefore allow us to estimate the size of the suppressive field. Defining size as the diameter corresponding to half of the total volume, we find that

on average the suppressive field is 2.0 ± 0.2 (s.e., bootstrap estimate, $n = 34$) times larger than the center of the RF (Figure 3F). These estimates are consistent with earlier measures based only on response gain (Bonin et al., 2005).

As in previous work, we postulate that local contrast is computed from the output of the light adaptation stage and is combined across a number of neurons (subunits) having spatially displaced RFs (Bonin et al., 2005; Shapley and Victor, 1979). The outputs of the subunits are squared and combined in a weighted sum, and the result is square rooted (Bonin et al., 2006). The weights are given by the profile of the suppressive field (Figure 3A). Because the responses of the subunits are shaped by light adaptation, which has a divisive effect on the responses, at steady state this computation of local contrast reduces to the common definition of root-mean-square contrast (Shapley and Enroth-Cugell, 1984), the ratio between the standard deviation and the mean of the local luminance distribution (Experimental Procedures).

Temporal Dynamics of Fast Adaptation

Finally, to apply the model to arbitrary scenes, we must specify how the signals driving the adaptation mechanisms are integrated over time. This matter has been extensively studied, and based on the literature we made two assumptions. First, we assumed that the measure of local luminance extends over ~100 ms in the recent past (Enroth-Cugell and Shapley, 1973a; Lankheet et al., 1993a; Lee et al., 2003; Saito and Fukada, 1986; Yeh et al., 1996). Second, we assumed that the measure of local contrast is determined entirely by the responses of the subunits, with no further temporal integration. Thus, the measure of local contrast is estimated over a brief interval (Alitto and Usrey, 2008; Baccus and Meister, 2002; Victor, 1987), whose duration is shorter when local luminance is high, and longer when local luminance is low.

The model is now complete (Figure 3A) and is general enough to be applied on arbitrary sequences of images. To gain an intuition for its operation, consider its responses to an increase in luminance (Figure S3). If mean luminance is suddenly increased while contrast is maintained constant, LGN neurons barely change their firing (Mante et al., 2005). Much of this invariance in the responses is due to light adaptation: after luminance is increased, a corresponding conductance increase in the light adaptation RC stage reduces the gain of the neuron. Light adaptation, however, is not instantaneous and cannot entirely suppress the stimulus-evoked transient. This transient is suppressed by the contrast gain control stage: the transient response of the subunits computing local contrast briefly increases the conductance of this RC stage. Surprisingly, therefore, the contrast gain control stage helps achieve seamless light adaptation. Thus, while increases in luminance and contrast have independent effects on the responses to steady-state stimuli (Mante et al., 2005), the underlying fast adaptation mechanisms show a marked interdependence in the response to transient stimuli.

Fitting the Responses to Simple Stimuli

To validate the model quantitatively and to estimate its parameters, we applied it to responses to simple grating stimuli varying in luminance and contrast (Figure S4). We have seen that these data can be explained by two RC stages in which the conductances are fixed for each stimulus condition based on prior knowledge of the stimulus (Figure 2). Here we ask if they can be fit by the complete model in which conductances are calculated dynamically from the time-varying images (Figure 3A). Success is not guaranteed because the conductances vary over time, and because the signals that set the conductance of the contrast gain control stage depend on the conductance of the light adaptation stage (Figure 3A).

The model provided excellent fits, accounting for 79% of the stimulus-driven variance (median, $n = 30$). This performance is indistinguishable from that of the earlier model in which the conductances were fixed to constant values on the basis of external knowledge (80% of the variance, Figure S4).

Predicting the Responses to Complex Stimuli

We then asked how the model performs when confronted with much more complex, naturalistic stimuli (Figures 4A–4D). We presented four sets of naturalistic sequences. The first was recorded by a camera mounted on the head of a cat roaming through a forest (methods described in Kayser et al. [2003]; <http://www.cogsci.uni-osnabrueck.de/~NBP/>) ("Cat-Cam," Movie S1). The second consisted of short sequences from a cartoon (Disney's *Tarzan*). The third and fourth are modified versions of the first set, scaled to have lower contrast or higher contrast than the original (at constant mean luminance). Examples of movies and LGN responses can be seen at <http://www.carandinilab.net/LGN>. Taken together, these sequences span a substantial range of contrast and luminance levels (Figures 4E–4H).

When we applied the model to these complex sequences, we found that its predictions closely resemble the measured responses (Figures 4A–4D). The model explains 65% of the stimu-

lus-driven variance in the measured responses for the example cell, and 59% (median) over the entire population (Figure 4M, horizontal axis). This performance is remarkable, considering that these are predictions, not fits; most of the model parameters are frozen, they are the same that we had obtained from the responses to drifting gratings. Thus, the mechanisms determining LGN responses operate similarly under both artificial and natural stimulation conditions.

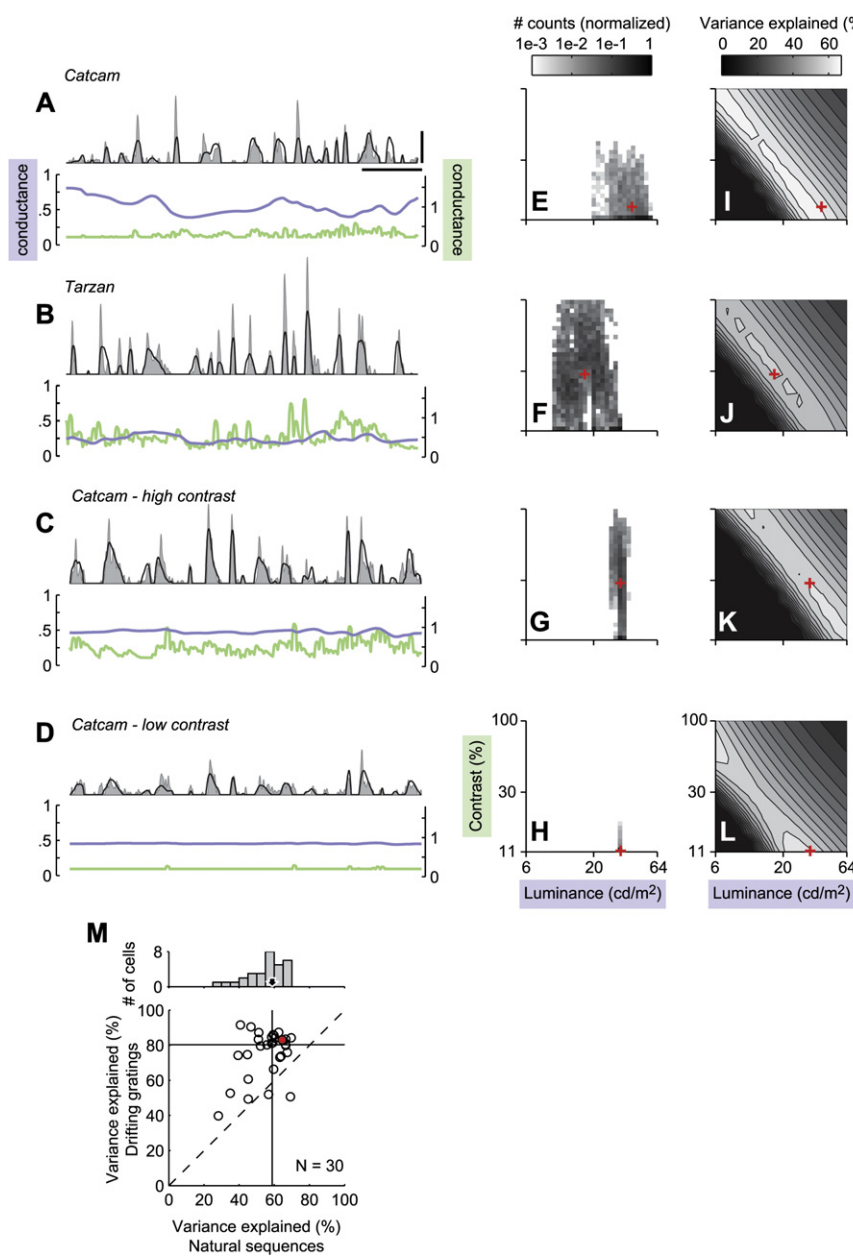
The model predictions are, however, less accurate for naturalistic sequences than for the drifting gratings (59% versus 80% explained stimulus-driven variance, Figure 4M). A drop in fit quality is to be expected given that model parameters were optimized for the responses to drifting gratings and not for the naturalistic sequences. However, an additional factor might be at play: the natural images are more complex in the spatial and temporal domain than the drifting gratings, and the model might be an incomplete description of the responses under these conditions.

To gauge the importance of this factor, we compared model performance on the naturalistic sequences to the performance on a third set of stimuli, which is intermediate between drifting gratings and naturalistic sequences (Figure 5). These stimuli are rapid sequences of flashed gratings of random spatial phase, spatial frequency, and orientation (Ringach et al., 1997). Spatially, these stimuli are identical to the drifting gratings, but temporally they contain a wider range of frequencies. The model performed equally well for the grating sequences as for the naturalistic sequences. The model explained 61% of the stimulus-related variance in the responses to the grating sequences (median, $n = 30$), lower than the 80% seen with drifting gratings (Figure 5B), but similar to the 59% seen with naturalistic sequences (Figure 5C).

The similar quality of model performance observed with flashed gratings and natural stimuli suggests that model shortcomings observed with these two types of stimuli might share a common origin. In particular, we investigated two possibilities. First, the shortcomings might reflect inadequacies in the model's accounting for the effects of fast adaptation in complex images. Second, the shortcomings might reflect additional nonlinear mechanisms that we have not included in the model.

Fast Adaptation in Responses to Complex Stimuli

We first asked whether the model captures the effects of fast adaptation in the responses to our naturalistic sequences. In these stimuli, the largest changes in luminance and contrast are seen across sequences rather than within sequences (Figures 4E–4H). Accordingly, the model's estimates of local luminance and local contrast vary considerably across sequences, and only moderately (though significantly) within sequences (Figures 4A–4D, bottom). It is therefore meaningful to ask whether for each sequence the model was able to identify the average weighting function that would optimally describe the responses. To find the optimal weighting function, we predicted the responses to each sequence with every temporal weighting function that can be generated by the model for a given neuron. We parameterized this space of weighting functions by the corresponding combinations of luminance and contrast (as in Figure 1B). We assessed their optimality by comparing how

**Figure 4. Responses to Natural Stimuli**

(A–D) Responses of an LGN neuron (gray) to four naturalistic movies and predictions (black) of the model (Figure 3A). Local luminance and local contrast and the associated conductances (blue and green) vary both within and across the movies. Scale bars, 500 ms and 100 spikes/s.

(E–H) The joint distributions of local luminance and local contrast for each of the four movies, and the corresponding averages (red crosses).

(I–L) Quality of predictions for different choices of a fixed RF (i.e., without fast adaptation), computed for each of the four movies. Each point corresponds to the prediction based on the RF estimated at a given luminance and contrast (same ranges as in Figure 1B). The subset of the RFs resulting in good predictions (brightest contour) differs across movies, reflecting their different average local luminance and local contrast (red crosses, redrawn from [E]–[H]).

(M) Quality of predictions of the model for responses to naturalistic sequences (horizontal axis) and drifting gratings (vertical). Filled lines and arrow are medians of distributions. The example neuron is drawn in red.

This ability of the model to select the appropriate RF for each sequence is critical, because no single, fixed RF is appropriate for all sequences. For the example neuron, any fixed RF could account for 0%–54% of the overall stimulus-driven variance in the responses. The upper bound will be reached with the fixed RF whose weighting function corresponds to the mean average luminance and contrast of all the naturalistic sequences. Thus, the model does better than any fixed RF could do and does so without any a priori knowledge of the luminance and contrast of the stimulus.

Indeed, a more detailed comparison between the model predictions and the predictions of the optimal, fixed RF

shows that the model corrects some of the shortcomings of the fixed RF (Figure 6). When the fixed RF underestimates the measured responses (Figure 6A, right half) the model appropriately predicts stronger responses, and when the fixed RF overestimates the responses (left half) the model appropriately predicts weaker responses. However, if the model perfectly corrected the errors of the fixed RF, then the data points would lie on the unity line. The points tend to fall between the unity line and the horizontal axis, which means that the model undercompensates for these errors. This effect is seen mostly in the responses to natural images: the same analysis on the response to drifting gratings of various mean luminances and contrasts yields points lying much closer to the unity line (Figures 6C and 6D).

well the corresponding predictions explain the responses (Figures 4I–4L).

The model typically succeeded in delivering the best temporal weighting functions among the ones it can produce. Only a subset of these weighting functions result in good predictions; this subset often corresponds to a contour with negative slope, because the effects of increasing luminance can be approximately compensated by decreasing contrast (Figures 4I–4L). The weighting functions generated by the model (Figures 4E–4L, red dots) invariably fell near this optimal subset. For the example cell (Figures 4I–4L, red), the optimal weighting functions explain 67% of the variance over all sequences (57% over the population, median), which is comparable to the fraction explained by the model itself (65% and 59%).

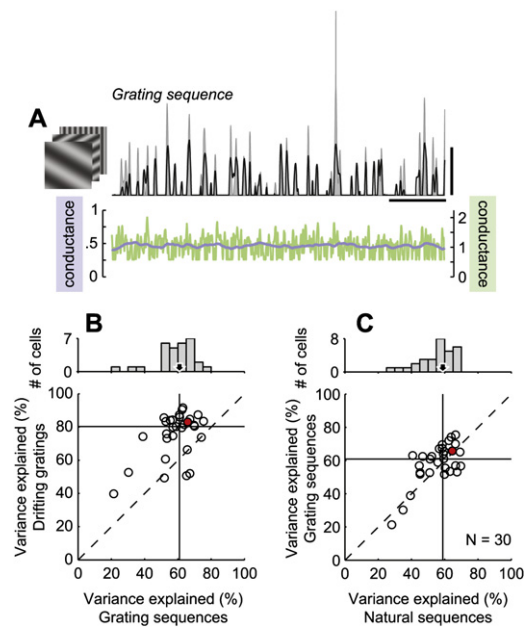


Figure 5. Responses to Grating Sequences

Stimuli are sequences of flashing gratings of random spatial frequency, spatial phase, and orientation.
 (A) Responses of an LGN neuron (gray, same neuron as in Figure 4), predictions of the model (black, Figure 3A), and the corresponding conductance of light adaptation (blue) and contrast gain control (green). Scale bars, 500 ms and 100 spikes/s.
 (B) Quality of predictions of the model for responses to grating sequences (horizontal axis) and drifting gratings (vertical). The filled lines and arrow are medians of distributions. The example neuron is drawn in red.
 (C) Quality of predictions of the model for responses to naturalistic sequences (horizontal axis) and grating sequences (vertical). Same format as in (B).

Additional Nonlinear Mechanisms

The inadequacies of the model are most pronounced at short time scales, i.e., at high temporal frequencies (Figure 7). Specific-

ically, the predicted responses contain less power at high frequencies than the measured responses (Figure 7A,C, compare black and blue). Indeed, the predicted time courses are less transient than the measured ones (Figures 4A–D). The model correctly predicts the phase in the measured responses up to about 25 Hz (Figures 7B and 7D), which is the frame rate at which we presented the naturalistic sequences; above this frequency the predictions tend to lead the measured responses. This phase difference, however, has little effect on the quality of predictions, as these contain only little power at these frequencies (Figures 7A and 7C). Removing these frequencies from the time courses has little effect on the average responses (Figures 7E–G). Similar observations can be made on the actual and predicted responses to artificial stimuli (Figure S5).

Several of the mechanisms that we have not incorporated into the model could contribute to these shortcomings. In particular, we tested the possible impact of two such mechanisms: a mechanism of burst generation (Lesica and Stanley, 2004; Mukherjee and Kaplan, 1995; Sherman, 2001; Smith et al., 2000) and a mechanism of slow adaptation (Baccus and Meister, 2002; Demb, 2002; Solomon et al., 2004).

Adding to the model a bursting mechanism would likely improve the model performance, at least for some neurons (Figure 8). On average over the population, 12% (median) of all spikes generated during the responses to naturalistic sequences occur as part of a burst, though the degree of burstiness varies substantially across neurons (Figure 8A). We found no clear correlation between the burstiness of a neuron and the quality of the corresponding model predictions (Figure 8A), but we did obtain the best predictions (percentage of stimulus-driven variance > 60%) for neurons with the least bursts (spikes in bursts < 21% of the total spikes). Moreover, the impact of burstiness on model performance can be shown clearly on a cell-by-cell basis by taking advantage of the variability of burstiness across trials (Figure 8B). The measured responses are better predicted by the model on trials with few bursts (60% stimulus-driven

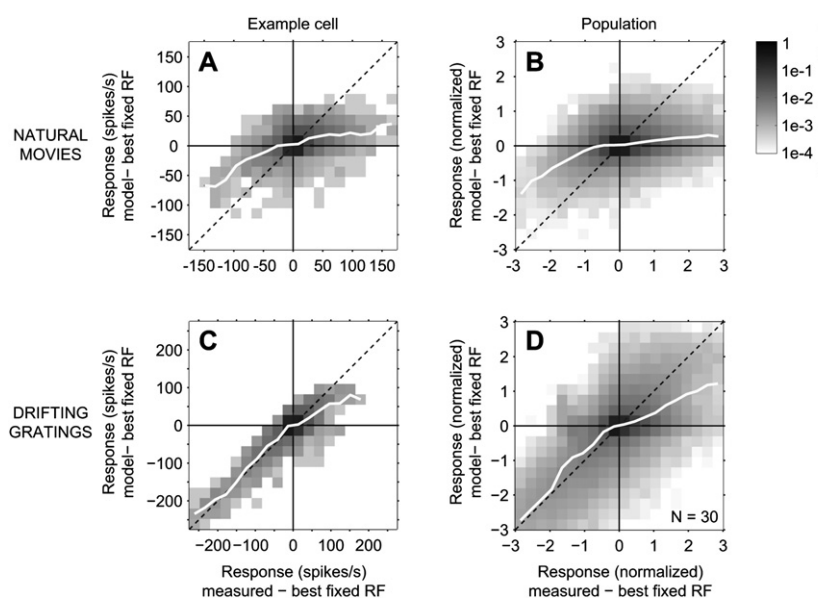


Figure 6. Model Validation

The model of fast adaptation (Figure 3A) partially corrects the shortcomings of a fixed linear RF.
 (A and B) Model validation on the responses to natural sequences.

(A) Joint histogram of deviations between the measured responses and the responses predicted by the fixed RF (horizontal axis) and between the responses predicted by the model and those predicted by the fixed RF (vertical axis). The fixed linear RF was optimized from the pooled responses to all naturalistic sequences. The average deviations between the model and the fixed RF are drawn in white and were computed over all bins sharing the same location along the horizontal axis. Same neuron as in Figure 4.

(B) Average histogram over the entire population of neurons.

(C and D) Model validation on responses to drifting gratings. Same format as in (A) and (B). The drifting gratings varied in luminance and contrasts (as in Figure 1B). The fixed RF was estimated with gratings of intermediate luminance and contrast.

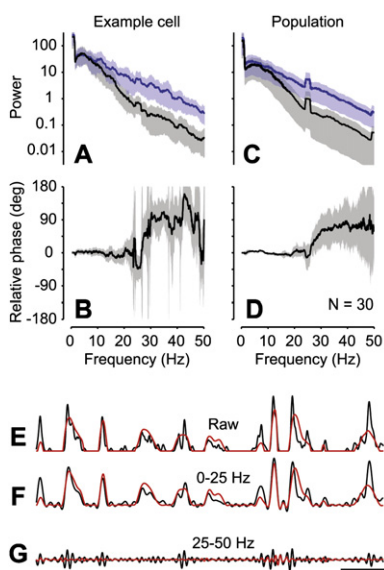


Figure 7. Frequency Analysis of Model Performance on Natural Sequences

(A) Power in the responses of an LGN neuron to natural sequences (blue) and in the corresponding predictions of the model (black, Figure 3A).

(B) Phase difference between the measured and predicted responses. (A and B) Averages over all movie sequences (line) \pm 1 SD (shading), same neuron as in Figure 4.

(C and D) Averages over the population (lines) \pm 1 SD (shading).

(E) Response of the example neuron (black) and predictions of the model (red) for a representative segment of a natural sequence.

(F) Low-frequency components in the measured (black) and predicted (red) responses for the same segment as in (E). Responses in (F) were filtered between 0 and 25 Hz, corresponding to frequencies below the frame rate of the natural movies.

(G) High-frequency components in the measured (black) and predicted (red) responses for the same segment as in (E). Responses in (G) were filtered between 25 and 50 Hz, corresponding to frequencies above the frame rate of the natural movies. Scale bars, 250 ms (horizontal) and 100 spikes/s (vertical).

variance explained and 6% of spikes occurring in bursts, median values) than on trials with many bursts (54% variance explained, 14% spikes in bursts).

Conversely, adding to the model a mechanism of slow adaptation would be unlikely to improve the predictions (Figure 9). We estimated the impact of slow adaptation by measuring

responses not only to the original natural sequences (Figure 9A, black) but also to modified movies (red), in which the first 6 s have been replaced by a blank screen. We compared the responses to the original and modified movies during a 2 s test period following the 6 s adaptation period. Responses in the two conditions are indistinguishable both for the example cell (Figure 9B) and over the entire population of neurons (Figure 9C). Total linear regression yields slopes of 1.01 ± 0.04 (95% confidence interval, bootstrap estimate) for the example cell and 0.99 ± 0.01 for the population, and intercepts of -0.01 ± 0.07 and 0.02 ± 0.01 . In another test of the similarity of the responses, we used the average responses to half of the trials of the original movies to predict the responses during the other half of the trials of the same movies (Figure 9D, horizontal axis) or of the corresponding modified movies (vertical axis). On average over all neurons, these two predictions explained the same fraction of stimulus-driven variance in the responses (the average difference between the corresponding fractions is $0.01\% \pm 0.01\%$, SE). Thus, slow adaptation is unlikely to be shaping the responses to the naturalistic sequences.

DISCUSSION

We have presented a general model of how LGN neurons respond to visual stimulation. The model operates on arbitrary image sequences and bridges an important gap by relating past studies that employed laboratory stimuli to more recent work that employed natural stimuli. Despite the growing literature on responses to natural stimuli, few studies could quantitatively relate their findings to the vast amount of data obtained using laboratory stimuli (Felsen and Dan, 2005; Rust and Movshon, 2005). A crucial achievement of the model is that it correctly captures how the RF is shaped by light adaptation and contrast gain control in response to natural stimuli. This represents a key step toward a complete model of LGN responses.

Our approach was to use simple stimuli to constrain most of the model's parameters, and to then keep these parameters fixed when predicting responses to more complex stimuli such as natural movies. A similar approach was taken in a seminal study by Dan et al. (1996). These authors defined a model that works on arbitrary image sequences (a spatiotemporal linear RF), found the parameters of that model with simple laboratory stimuli (white noise), and applied the model to naturalistic stimuli

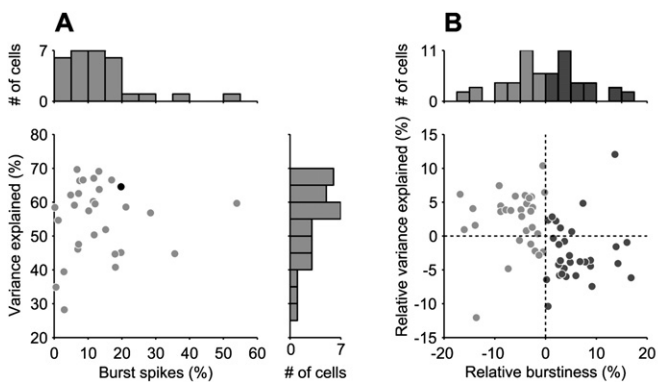
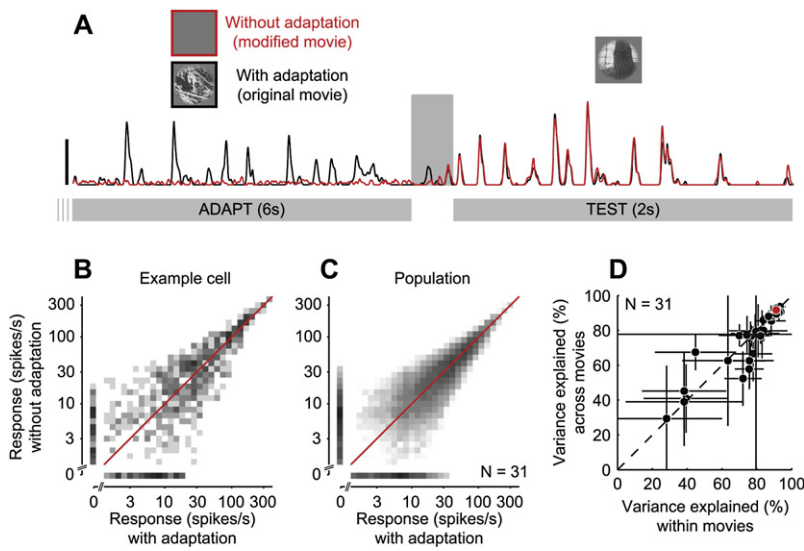


Figure 8. Impact of Bursting on Model Predictions

(A) Relation between the average burstiness of LGN neurons in the responses to natural sequences (horizontal axis) and the quality of the corresponding model predictions (as in Figures 4A–4D, black) (vertical axis). For each neuron, burstiness is the ratio of the number of spikes occurring in bursts over the total number of spikes. The example neuron of Figure 4 is drawn in black.

(B) Quality of model predictions on trials with few bursts (light gray) and many bursts (dark gray). Relative burstiness (horizontal axis) and relative quality of predictions (vertical axis) are computed by subtracting the burstiness and quality of predictions computed over all trials from the values computed across the two subsets of trials. Each neuron corresponds to two points (i.e., high and low burstiness) in symmetric positions with respect to the origin. Histograms (top and right) are marginal distributions computed separately for trials with many (dark gray) and few (light gray) bursts.



(the film *Casablanca*). This work was the very first step in the direction that we advocate. We have provided a second step by testing a model that greatly extends a simple linear RF, which we endowed with fast adaptation mechanisms.

With few parameters, the model captures the amplitude and the time course of the responses to gratings of different mean light levels, contrasts, sizes, temporal frequencies, and spatial frequencies. Moreover, the model predicts much of the responses to complex, rapidly changing stimuli, down to a time scale of about 20 ms (the sampling interval required to measure responses to 25 Hz). Specifically, the model captures how these responses are affected by changes in luminance and contrast level, overcoming many of the shortcomings of simpler models.

Our results indicate that the main effects of light adaptation and contrast gain control are similar under laboratory and natural stimulation conditions. Nonlinear mechanisms may operate differently for different classes of stimuli (Olshausen and Field, 2005), and it is reassuring to find that this is not the case for two such important mechanisms. Indeed, the model performed as well on complex naturalistic images as it did on sequences of gratings and was consistently able to yield a close-to-optimal RF in the face of sequences with substantial variations in luminance and contrast, without the need for introducing prior knowledge about the statistics of the stimulus.

However, we may also have found some evidence for differences in the operation of fast adaptation with artificial and natural stimuli: for natural stimuli but not for gratings, the model undercompensates the errors of a fixed linear RF (Figure 6). These differences might reflect changes in the spatial profile of the RF with stimulus type. The spatial profile of the RF in our model is fixed; the responses of the RF center and surround are equally affected by the adaptation mechanisms. This assumption is consistent with the finding that the tuning of ganglion cell responses for spatial frequencies is independent of the mean luminance (Troy et al., 1999). It is also consistent with the finding that the tuning of LGN responses for spatial

Figure 9. Lack of Slow Adaptation in the Responses to Naturalistic Sequences

(A) Measured responses to a segment of a naturalistic sequence. Responses to the original movie (black) are compared to responses to modified movie (red), in which the first 6 s (adapt) have been replaced by a blank screen. Same neuron shown in Figure 4. Scale bar, 100 spikes/s. (B) Joint histogram of responses to the original and modified movies during the test period, starting 250 ms after the end of the adaptation period (adapt) and lasting 2 s. Red line is the unity line. Same neuron as in (A). (C) Average over the entire population of neurons ($n = 31$). (D) Similarity of responses to the original and modified movies during the test period, assessed by trying to predict one based on the other. We used the average responses to half (typically five) of the trials of the original movies to predict the responses during the other half of the trials of the same movies (horizontal axis) or of the corresponding modified movies (vertical axis). Circles and error bars are medians and SD of the stimulus-driven variance explained by the predictions, computed over all possible ways to subdivide all trials into two groups. The example cell (A and B) is drawn in red.

frequencies is independent of stimulus contrast (Bonin et al., 2005) and is supported by the very success of the model at predicting the responses to gratings of various contrasts and sizes (Figure 3). Nonetheless, recent evidence suggests that the effects of contrast gain control on RF center and surround are mediated by different mechanisms (Beaudoin et al., 2007); it is therefore possible that contrast gain control affects the RF center and surround differently.

These differences seen in LGN with artificial and natural stimuli may contribute to related effects observed in the next stage of visual processing, the primary visual cortex (V1). The RF of V1 neurons was found to vary with the type of stimulus used (David et al., 2004; Sharpee et al., 2006), and similar results were seen in the neurons' responsiveness (Felsen et al., 2005; Smyth et al., 2003). As a result, models of V1 responses constrained with artificial stimuli may not perform well when tested on natural stimuli (David et al., 2004; Olshausen and Field, 2005; Weliky et al., 2003).

To define the model of contrast gain control, we drew on previous work that defined and quantified a divisive “suppressive field,” a mechanism that computes a local measure of contrast and operates divisively on the output of the RF (Bonin et al., 2005, 2006). Here we posited that this division is obtained by increasing the conductance of the contrast gain control RC stage. We confirmed the validity of this choice by showing how increasing the size of a grating decreases not only the RF's gain but also the RF's integration time, exactly in the same way as a matched increase in contrast (Figure 3). To restate this result in terms of much of the existing literature, our model correctly predicted that “size tuning” (or “surround suppression”) should operate by the same mechanism as “contrast saturation”: both in terms of gain and of integration time, an increase in contrast was indistinguishable from an increase in size. Because at steady state it reduces to the earlier divisive model, the present model also predicts well-known nonlinear properties of LGN responses: not only “contrast saturation” and “size tuning” as shown here,

but also “masking” and “surround suppression” (Bonin et al., 2005).

The goal of our model is to provide a functional account of LGN responses, not a biophysical description. The model relies on RC circuits because their effects are intuitive and they provide an excellent account for the data. However, its success should not be taken as support for the obvious biophysical interpretation of these RC circuits, which involves the membrane conductance of LGN or retinal neurons. The effects of fast adaptation could arise from many alternative biophysical mechanisms. For example, our RC model is mathematically similar to an earlier account of contrast gain control in the retina based on high-pass filters (Shapley and Victor, 1981); this model in turn suggests a different biophysical interpretation. Current research in retina is making steady progress in identifying the biophysical mechanisms underlying fast adaptation and is illuminating their variety (e.g., Beaudoin et al., 2007; Dunn et al., 2007).

To improve the model’s predictions, especially at fine time scales, the most valuable addition would be a spiking mechanism, possibly one capable of bursts. In our model, firing rates are modeled as rectified membrane potentials, an approximation which is accurate at time scales down to tens of milliseconds (Carandini and Ferster, 2000). At shorter time scales, the responses are more affected by the spike generation mechanism. In particular, we have shown that the presence of spike bursts has a detrimental effect on model predictions (Figure 8). These are thought to be more prominent in responses to natural stimuli (Denning and Reinhagel, 2005; Lesica and Stanley, 2004; Wang et al., 2007), and therefore accounting for them should improve model predictions. We have concentrated our efforts on the fast adaptation mechanisms, whose effects on the responses to naturalistic stimuli involve stages of image processing. Adding an appropriate spike mechanism to the model, however, may not be trivial. Models that successfully predict individual-spike responses have thus far been limited to a simple linear front end (Keat et al., 2001; Pillow et al., 2005). Constraining the parameters of a spiking model with a nonlinear front end is a major computational challenge.

The model might be further improved by testing a number of novel predictions. For instance, the model predicts that at high temporal frequencies local contrast increasingly reflects not only the root-mean-square contrast of the stimulus, but also its mean luminance (Figure S4). Similarly, steps in mean luminance are predicted to engage contrast gain control in addition to light adaptation, even when the spatial root-mean-contrast of a stimulus remains constant (Figure S3). Disentangling these effects in neurons will be challenging, and most likely will be possible only with appropriately chosen artificial stimuli.

Similarly, much could be learned by testing the model on a wider array of natural stimuli. Obviously, our naturalistic sequences represent only a small subset of possible natural stimuli. The model may perform better or worse for different classes of natural stimuli. In particular, the contributions of the various nonlinear mechanisms discussed above (i.e., fast adaptation, bursting, and slow adaptation) might vary considerably across different natural stimuli.

Finally, the model should be extended to account for other cell types. The model was designed to account for the responses of

X cells, which correspond to 50% of retinal ganglion cells in the cat (Masland, 2001; Rodieck et al., 1993; Wassle, 2004). The model does not account for additional nonlinearities present in the responses of Y cells. Since Y-type responses are thought to be mediated by subunits similar to those computing local contrast (Enroth-Cugell and Freeman, 1987; Hochstein and Shapley, 1976a; Victor and Shapley, 1979), it might be straightforward to extend the model to capture also those nonlinearities. This would most likely result in better predictions for a minority of cells in our sample.

Even though our model does not capture the operation of all known nonlinear mechanisms, it promises to be a useful tool to understand the computations performed by the early visual system. Fast adaptation in the retina and LGN are likely to affect also later stages of visual processing, and indeed similar putative effects of fast adaptation have been found along the hierarchy of visual areas (Carandini et al., 2005). By using the model as a building block in cascaded models of the visual system (Rust et al., 2006), it will be possible to disentangle computations performed by the later stages from those already implemented in the retina and LGN. Moreover, given that the model can be applied to arbitrary stimuli, it can serve as a “null hypothesis” that might explain additional, possibly yet to be discovered, nonlinear phenomena that are not obviously related to fast adaptation. Finally, a general model of fast adaptation will be invaluable to test specific hypotheses (Laughlin, 1981; Schwartz and Simoncelli, 2001; Van Hateren, 1993) about the function of adaptation in natural vision.

EXPERIMENTAL PROCEDURES

Here we describe the experimental procedures and the model that we applied to the data. A more intuitive explanation of the model is given in the **Results**; a careful explanation of parameter fitting is given in the **Supplemental Experimental Procedures**.

Physiological Recordings

Adult cats were anesthetized with ketamine (20 mg/kg) mixed with acepromazine (0.1 mg/kg) or xylazine (1 mg/kg). Anesthesia was maintained with a continuous intravenous infusion of pentothal (0.5–4 mg kg⁻¹ h⁻¹). Animals were paralyzed with pancuronium bromide (0.15 mg kg⁻¹ h⁻¹) and artificially respiration with a mixture of O₂ and N₂O (typically 1:2). EEG, electrocardiogram, and end-tidal CO₂ were continuously monitored. The Animal Care and Use Committee of the Smith-Kettlewell Eye Research Institute approved all procedures.

A craniotomy was performed above the right LGN (Horsley-Clarke ~A6L9). The location of LGN was determined from the sequence of ocular dominance changes during penetration. Extracellular signals were recorded with Quartz-coated Platinum/Tungsten Microelectrodes (Thomas Recording, Giessen, Germany). Firing rates were obtained by convolving spike trains with a Gaussian window (SD 5 ms).

Visual stimuli were displayed using the Psychophysics Toolbox (Brainard, 1997; Pelli, 1997) and presented monocularly on a calibrated CRT screen with mean luminance of 32 cd/m² and refresh rate of 125 Hz, placed typically at a distance of 57 cm. Stimuli lasted 0.5–17 s and were presented in blocks of 3 to 15 repeats. Stimuli within blocks were presented in randomized order. Each block included one or more blank (gray) stimuli.

We used three kind of stimuli: drifting gratings, complex naturalistic stimuli (“CatCam” and Tarzan movies), and complex artificial stimuli. The CatCam movies were collected as part of a project by Peter König’s laboratory (<http://www.cogsci.uni-osnabrueck.de/~NBP/>). All movies were presented through a circular window extending beyond the borders of the receptive field

and had a refresh rate of 25 Hz. The movies differed in their mean luminance and contrast. For instance, the four example movies discussed in the [Results](#) have an average mean luminance of 40 (CatCam), 15 (*Tarzan*), and 32 cd/m² (low and high contrast) and an average spatial root-mean-square-contrast of 26 (CatCam), 51 (*Tarzan*), 10 (low contrast), and 48% (high contrast). The complex artificial stimuli were sequences of flashed gratings with random spatial frequency (six to eight values), spatial phase (four values), and orientation (four to eight values) ([Ringach et al., 1997](#)).

We report on the responses of 49 neurons in the LGN of seven adult cats. Of these neurons, 22 were located in the first contralateral layer (presumably lamina A), 23 in the first ipsilateral layer (presumably lamina A_I), two in subsequent layers, and two were unclassified. We classified neurons into ON-center (30 cells) and OFF-center (19 cells) by mapping the RF with rapid sequences of flashed gratings ([Ringach et al., 1997](#)). We classified neurons into X type (41 cells) and Y type (8 cells) based on standard criteria ([Hochstein and Shapley, 1976b](#)). The eccentricity of the RF ranged between 2.2° and 19.9° for 80% of the cells, with a median of 10.3°.

Quality of Fits

Unless otherwise stated, fits minimize square error between measured responses and model predictions. Square error is given by $\sum_{ij} (m_{ij} - r_j)^2$ where m_{ij} denote the observed response to trial i of stimulus j , and r_j represent the response predicted by the model.

To quantify how well the model predictions r_t capture the measured responses m_t (both consisting of $t = 1, \dots, M$ samples) we estimated the fraction of stimulus-driven (accountable) variance in the responses accounted for by the model ([Machens et al., 2004; Sahani and Linden, 2003](#)):

$$\beta = \frac{\sigma_m^2 - \sigma_e^2}{\sigma_m^2 - \sigma_\eta^2}$$

where:

$$\sigma_m^2 = \left\langle \frac{1}{M} \sum_t m_t^2 \right\rangle$$

is the power in the response (assuming zero mean),

$$\sigma_e^2 = \left\langle \frac{1}{M} \sum_t (r_t - m_t)^2 \right\rangle$$

is the mean square distance between data and model, and

$$\sigma_\eta^2 = \frac{d}{d-1} \left[\left\langle \frac{1}{M} \sum_t m_t^2 \right\rangle - \frac{1}{M} \sum_t \langle m_t^2 \rangle \right]$$

is an estimate of the variance in m_t that is due to noise. Angular brackets indicate the average over d presentations of the same stimulus. A perfect model is one that yields $\beta = 1$, or 100%, while $\beta = 0$ indicates that a constant value would have been better than the proposed model.

Model Definition

The input to the model ([Figure 3A](#)) is an arbitrary luminance distribution $s(x,y,t)$, and its output is the time-varying firing rate $r(t)$. The model consists of six consecutive stages: (1) a fixed linear filter, (2) light adaptation, (3) subtractive adaptation, (4) contrast gain control, (5) a fixed temporal filter, (6) rectification.

Linear Filtering

The first stage yields the convolution $r_{lin}(t)$ of the fixed linear filter $h_{lin}(x,y,t)$ and the stimulus $s(x,y,t)$:

$$r_{lin}(t) = [h_{lin} * s](x_0, y_0, t), \quad (1)$$

where x_0, y_0 are coordinates of the filter center. The filter has a center-surround organization:

$$h_{lin}(x,y,t) = q_c(x,y)f_{lin}(t) - \mu_s q_s(x,y)f_{lin}(t - \delta),$$

where q_c and q_s are Gaussians of widths η_c and η_s and unity volume, μ_s is the surround strength, δ is the delay between center and surround, and $f_{lin}(t)$ is the

temporal weighting function, given by a difference of Gamma functions $u_i(t)$ ([Cai et al., 1997](#)):

$$f_{lin}(t) = p \cdot [u_1(t) - ku_2(t)], \quad k \geq 0 \quad (2)$$

where p sets the amplitude of the filter and

$$u_i(t) = |t - \kappa|^\alpha \exp\left(-\frac{|t - \kappa|}{\phi_i}\right) \quad (3)$$

with $\phi_i, \kappa > 0, |\cdot|$ indicating rectification, and $j = 1, 2$. We imposed $\phi_1 > \phi_2$, to ensure a physiologically plausible shape of $f_{lin}(t)$.

Light Adaptation

The second stage consists of a batch of n_L RC circuits in series which capture the effects of light adaptation. For $n_L = 1$, response r_{lum} is computed by solving:

$$\frac{d}{dt} r_{lum}(t) = \frac{1}{C_L} (r_{lin}(t) - g_L(t)r_{lum}(t)), \quad (4)$$

where capacitance C_L is fixed for a given neuron and conductance g_L depends on stimulus luminance. For the neurons in our sample, n_L is typically > 1 and r_{lum} is obtained by solving Equation 4 n_L times. In this case, only the conductance of the first RC circuit depends on luminance; for all other RC circuits we set $g_L = 1$. The capacitance of the n_L RC circuits is chosen such that all have the same time constant $\tau_L = C_L/g_L$.

The conductance g_L is proportional to a measure of local luminance L_{Local} :

$$g_L(t) = \alpha L_{Local}(t) \quad (5)$$

Local luminance $L_{Local}(t)$ is computed by integrating stimulus luminance over a small region of space and a short interval of time:

$$L_{Local}(t) = [h_{la} * s](x_0, y_0, t), \quad (6)$$

with

$$h_{la}(x, y, t) = q_s(x, y)f_{la}(t),$$

that is we set the spatial profile of the light adaptation filter to be identical to the surround of the fixed linear filter.

The temporal profile of the filter is a Gamma function:

$$f_{la}(t) = |t|^\alpha \exp\left(-\frac{|t|}{\phi_{la}}\right)$$

with $\phi_{la} = 35$ ms for all neurons.

Subtractive Adaptation

To simplify the operation of subsequent stages in the model, we redefine r_{lum} such that its steady-state value in response to a static, spatially uniform stimulus of luminance L is zero:

$$r_{lum}^*(t) \equiv r_{lum}(t) - \frac{1}{\alpha} \int h_{lin}(x_0, y_0, t) dx dy dt.$$

To make sure that the same is true also for a static stimulus with an arbitrary spatial luminance distribution, we define an additional, subtractive, adaptation stage:

$$r_{sa}(t) = r_{lum}^*(t) - [f_{sa} * r_{lum}^*](t),$$

where the responses after light adaptation are weighted by a Gamma function:

$$f_{sa}(t) = |t|^\alpha \exp\left(-\frac{|t|}{\phi_{sa}}\right)$$

with $\phi_{sa} = 200$ ms for all neurons.

Contrast Gain Control

The effects of contrast gain control are also captured by a batch of n_C RC circuits in series. For $n_C = 1$, the RC circuit has fixed capacitance C_C and a variable conductance g_C that depends on stimulus contrast, and is thus described by:

$$\frac{d}{dt} r_{con}(t) = \frac{1}{C_C} (r_{sa}(t) - g_C(t)r_{con}(t)) \quad (7)$$

For $n_C > 1$, we obtain r_{con} by integrating Equation 7 n_C times. As above, only the conductance of the first RC circuit depends on contrast; for all other RC circuits we set $g_C = 1$. The capacitance of the n_C RC circuits is chosen such that all have the same time constant $\tau_C = C_C/g_C$.

The conductance g_C depends on a measure of local contrast C_{Local} :

$$g_C(t) = [\beta C_{Local}(t)]^\gamma \quad (8)$$

We compute local contrast from the responses of a large population of subunits covering the RF of the LGN neuron (Bonin et al., 2005; Shapley and Victor, 1979). The processing performed by the subunits is identical to that performed by the LGN neuron except for a shift in RF position. The subunit centers are chosen to uniformly cover the RF of the LGN neuron. The distance Δx_{su} between neighboring subunits is:

$$\Delta x_{su} = \frac{\pi \cdot \eta_c}{2}$$

where $2\eta_c$ is the standard deviation of the RF center q_c . For each LGN neuron, we modeled the responses of 169 subunits, covering a 13×13 square grid.

Local contrast is then defined as:

$$C_{local}(t) = \sqrt{\sum_{i=1,N} q_{su}(x_i, y_i) \left(|r'_{sa}(t)|^2 + | - r'_{sa}(t)|^2 \right)} \quad (9)$$

Where the index i runs over all subunits, and the two terms in the summand correspond to a population of ON-center cells and a population of OFF-center cells. The subunits are weighted by a Gaussian q_{su} centered on the LGN RF. The size η_{su} of q_{su} is twice the size η_c of the RF center.

We conservatively imposed C_{local} to have a lower bound:

$$C_{local}(t) >= C_{min},$$

where for any given neuron C_{min} is the smallest contrast at which we estimated the temporal weighting function of the neuron.

Temporal Filtering

After contrast gain control, the responses are convolved with a second band-pass filter:

$$r_{bp}(t) = [f_{bp} * r_{con}](t) \quad (10)$$

where $f_{bp}(t)$ is a difference of Gamma functions (Equation 2).

Because of this second band-pass filter, the selectivity for temporal frequency of the LGN neuron differs from the selectivity of the subunits computing local contrast (Bonin et al., 2005).

Rectification

Finally, we obtain firing rates by rectifying the membrane potential:

$$r(t) = |r_{max}r_{bp}(t) + r_0| \quad (11)$$

where r_{max} sets the overall gain of the neuron and r_0 is the resting membrane potential.

Parameter Estimation

We separately constrained the stages of the model in a series of steps. In each step we fitted the model to responses to gratings whose attributes were tailored to isolate only one (or few) stages. Moreover, we didn't fit the full model (Figure 3A) to all these sets of responses, but rather at each stage resorted to the simplest implementation of the model that allowed us to explain the responses at hand. Having estimated the parameters of the model from the responses to gratings, we then use the model to predict the responses to natural stimuli. These procedures are described in detail in the Supplemental Experimental Procedures.

Model Validation

Predictions of the Fixed Linear RF

To compute the predictions of fixed linear RFs (Figures 4I–5L) we used the same parameters used to predict responses to natural sequences (Figures 4A–4D), while imposing that local luminance and local contrast be constant over time. The range of local luminance and local contrast applied matched that used to characterize the neurons (Figure 1B). We then determined the values of local luminance and local contrast yielding the best predictions. We either optimized local luminance and local contrast for each sequence separately or over all sequences at once. Each of the resulting pairs of local luminance and local contrast values corresponds to a fixed linear RF, which is optimal for a given sequence, or over all sequences at once.

Analysis of Errors

To validate the model, we compared its predictions to those of the optimal RF over all sequences (Figure 6). We computed the difference between the measured responses and the predictions of the optimal RF and compared the result to the difference between model predictions (Figure 6) and those of the optimal RF. We estimated the joint distribution of deviations by downampling responses to 100 Hz and binning the result with a 21×21 grid of linearly spaced bins. To compute the distribution across neurons, we normalized the responses of each neuron by the firing rate corresponding to the 95th percentile of its firing rate distribution over the duration of the natural sequences.

Frequency Analysis of Model Performance

To evaluate model performance at different time scales, we calculated the power spectrum $S_X(f)$ and the cross-spectrum $S_{XY}(f)$ between measured responses and model predictions (Bendat and Piersol, 2000):

$$S_X(f) = |X(f)|^2$$

$$S_{XY}(f) = Y(f)X^*(f)$$

where $X(f)$ and $Y(f)$ are the Fourier transforms of two continuous time series $x(t)$ and $y(t)$. We obtained estimates of these quantities via multitaper analysis (Mitra and Pesaran, 1999). We used 21 taper functions with time-bandwidth product $nw = 11$ and applied them to the responses measured over the entire length of a given stimulus.

To compute the power spectrum of the responses (Figures 7A and 7B), we set $x(t) = r_j(t)$ and $y(t) = m_j(t)$, where $r_j(t)$ and $m_j(t)$ are the predicted and measured responses for stimulus j :

$$m_j(t) = \langle m_{ij}(t) \rangle_i$$

and $m_{ij}(t)$ denote the observed response to trial i of stimulus j , and angular brackets indicate the average over d presentations of the same stimulus.

To compute the relative phase between measured and predicted responses we first obtained the phase of S_{XY} for each trial i by setting $x(t) = r_j(t)$ and $y(t) = m_{ij}(t)$ and then computed the circular average over all trials.

Effect of Bursting

Following standard criteria, we defined bursts as sequences of spikes preceded by at least 100 ms of silence (i.e., no spikes) and containing spikes separated by interspike intervals of 4 ms or less (Guido et al., 1992; Lu et al., 1992). The burstiness of responses (Figure 8) can then be defined as the percentage of spikes that are contained in a burst (Lesica and Stanley, 2004).

Effect of Slow Adaptation

We tested for the effects of slow adaptation by measuring responses to modified natural sequences (CatCam and Tarzan) in which the first 6 s were replaced by a blank screen. We analyzed responses falling into a 2 s temporal window starting 250 ms after the offset of the blank screen. The delay of 250 ms was used to avoid contamination of the responses by transients due to the sudden stimulus onset. To reduce the correlations across subsequent samples, for this analysis we downsampled the responses to 333 Hz. We then computed total linear regression between the responses to the two movies by finding the line with the smallest summed, squared, orthogonal distance to the data points. We used bootstrapping (Efron and Tibshirani, 1993) to find confidence intervals for the parameters of the best fitting line (1000 samples).

SUPPLEMENTAL DATA

The Supplemental Data for this article can be found online at <http://www.neuron.org/cgi/content/full/58/4/625/DC1/>.

ACKNOWLEDGMENTS

We thank Peter König for the use of the "CatCam" movies. Supported by a James S. McDonnell 21st Century Award in Brain, Mind, and Behavior.

Received: December 20, 2007

Revised: February 29, 2008

Accepted: March 14, 2008

Published: May 21, 2008

REFERENCES

- Alitto, H.J., and Usrey, W.M. (2008). Origin and dynamics of extraclassical suppression in the lateral geniculate nucleus of the macaque monkey. *Neuron* 57, 135–146.
- Baccus, S.A., and Meister, M. (2002). Fast and slow contrast adaptation in retinal circuitry. *Neuron* 36, 909–919.
- Baylor, D.A., Hodgkin, A.L., and Lamb, T.D. (1974). Reconstruction of the electrical responses of turtle cones to flashes and steps of light. *J. Physiol.* 242, 759–791.
- Beaudoin, D.L., Borghuis, B.G., and Demb, J.B. (2007). Cellular basis for contrast gain control over the receptive field center of mammalian retinal ganglion cells. *J. Neurosci.* 27, 2636–2645.
- Benardete, E.A., and Kaplan, E. (1999). The dynamics of primate M retinal ganglion cells. *Vis. Neurosci.* 16, 355–368.
- Bendat, J.S., and Piersol, A.G. (2000). *Random Data: Analysis and Measurement Procedures*, Third Edition (New York: Wiley).
- Bonin, V., Mante, V., and Carandini, M. (2005). The suppressive field of neurons in lateral geniculate nucleus. *J. Neurosci.* 25, 10844–10856.
- Bonin, V., Mante, V., and Carandini, M. (2006). The statistical computation underlying contrast gain control. *J. Neurosci.* 26, 6346–6353.
- Brainard, D.H. (1997). The psychophysics Toolbox. *Spat. Vis.* 10, 433–436.
- Brodie, S.E., Knight, B.W., and Ratliff, F. (1978). The spatiotemporal transfer function of the Limulus lateral eye. *J. Gen. Physiol.* 72, 167–202.
- Butts, D.A., Weng, C., Jin, J., Yeh, C.I., Lesica, N.A., Alonso, J.M., and Stanley, G.B. (2007). Temporal precision in the neural code and the timescales of natural vision. *Nature* 449, 92–95.
- Cai, D., DeAngelis, G.C., and Freeman, R.D. (1997). Spatiotemporal receptive field organization in the lateral geniculate nucleus of cats and kittens. *J. Neurophysiol.* 78, 1045–1061.
- Carandini, M., Heeger, D.J., and Movshon, J.A. (1997). Linearity and normalization in simple cells of the macaque primary visual cortex. *J. Neurosci.* 17, 8621–8644.
- Carandini, M., and Ferster, D. (2000). Membrane potential and firing rate in cat primary visual cortex. *J. Neurosci.* 20, 470–484.
- Carandini, M., Demb, J.B., Mante, V., Tolhurst, D.J., Dan, Y., Olshausen, B.A., Gallant, J.L., and Rust, N.C. (2005). Do we know what the early visual system does? *J. Neurosci.* 25, 10577–10597.
- Carandini, M., Horton, J.C., and Sincich, L.C. (2007). Thalamic filtering of retinal spike trains by postsynaptic summation. *J. Vis.* 7, 20.1–20.11.
- Cleland, B.G., and Enroth-Cugell, C. (1968). Quantitative aspects of sensitivity and summation in the cat retina. *J. Physiol.* 198, 17–38.
- Cleland, B.G., and Freeman, A.W. (1988). Visual adaptation is highly localized in the cat's retina. *J. Physiol.* 404, 591–611.
- Cohen, H.I., Christen, W.G., and Winters, R.W. (1981). Spatial summation of signals and adaptation by the surround response mechanism of cat retinal ganglion cells. *Exp. Brain Res.* 44, 207–212.
- Dahari, R., and Spitzer, H. (1996). Spatiotemporal adaptation model for retinal ganglion cells. *J. Opt. Soc. Am. A Opt. Image Sci. Vis.* 13, 419–435.
- Dan, Y., Atick, J.J., and Reid, R.C. (1996). Efficient coding of natural scenes in the lateral geniculate nucleus: Experimental test of a computational theory. *J. Neurosci.* 16, 3351–3362.
- David, S.V., Vinje, W.E., and Gallant, J.L. (2004). Natural stimulus statistics alter the receptive field structure of v1 neurons. *J. Neurosci.* 24, 6991–7006.
- Dawis, S., Shapley, R., Kaplan, E., and Tranchina, D. (1984). The receptive field organization of X-cells in the cat: Spatiotemporal coupling and asymmetry. *Vision Res.* 24, 549–564.
- Demb, J.B. (2002). Multiple mechanisms for contrast adaptation in the retina. *Neuron* 36, 781–783.
- Denning, K.S., and Reinagel, P. (2005). Visual control of burst priming in the anesthetized lateral geniculate nucleus. *J. Neurosci.* 25, 3531–3538.
- Dunn, F.A., Lankheet, M.J., and Rieke, F. (2007). Light adaptation in cone vision involves switching between receptor and post-receptor sites. *Nature* 449, 603–606.
- Efron, B., and Tibshirani, R.J. (1993). *An Introduction to the Bootstrap*, Volume 57 (New York: Chapman & Hall).
- Enroth-Cugell, C., and Shapley, R.M. (1973a). Adaptation and dynamics of cat retinal ganglion cells. *J. Physiol.* 233, 271–309.
- Enroth-Cugell, C., and Shapley, R.M. (1973b). Flux, not retinal illumination, is what cat retinal ganglion cells really care about. *J. Physiol.* 233, 311–326.
- Enroth-Cugell, C., Lennie, P., and Shapley, R.M. (1975). Surround contribution to light adaptation in cat retinal ganglion cells. *J. Physiol.* 247, 579–588.
- Enroth-Cugell, C., and Freeman, A.W. (1987). The receptive-field spatial structure of cat retinal Y cells. *J. Physiol.* 384, 49–79.
- Fain, G.L., Matthews, H.R., Cornwall, M.C., and Koutalos, Y. (2001). Adaptation in vertebrate photoreceptors. *Physiol. Rev.* 81, 117–151.
- Felsen, G., and Dan, Y. (2005). A natural approach to studying vision. *Nat. Neurosci.* 8, 1643–1646.
- Felsen, G., Touryan, J., Han, F., and Dan, Y. (2005). Cortical sensitivity to visual features in natural scenes. *PLoS Biol.* 3, e342. 10.1371/journal.pbio.0030342.
- Fuortes, M.G.F., and Hodgkin, A.L. (1964). Changes in the time scale and sensitivity in the ommatidia of Limulus. *J. Physiol.* 172, 239–263.
- Gaudiano, P. (1994). Simulations of X and Y retinal ganglion cell behavior with a nonlinear push-pull model of spatiotemporal retinal processing. *Vision Res.* 34, 1767–1784.
- Guido, W., Lu, S.M., and Sherman, S.M. (1992). Relative contributions of burst and tonic responses to the receptive field properties of lateral geniculate neurons in the cat. *J. Neurophysiol.* 68, 2199–2211.
- Hochstein, S., and Shapley, R.M. (1976a). Linear and nonlinear spatial subunits in Y cat retinal ganglion cells. *J. Physiol.* 262, 265–284.
- Hochstein, S., and Shapley, R.M. (1976b). Quantitative analysis of retinal ganglion cell classifications. *J. Physiol.* 262, 237–264.
- Kaplan, E., and Benardete, E. (2001). The dynamics of primate retinal ganglion cells. *Prog. Brain Res.* 134, 17–34.
- Kayser, C., Einhäuser, W., and Konig, P. (2003). Temporal correlations of orientations in natural scenes. *Neurocomputing* 52–54, 117–123.
- Keat, J., Reinagel, P., Reid, R.C., and Meister, M. (2001). Predicting every spike: A model for the responses of visual neurons. *Neuron* 30, 803–817.
- Lankheet, M.J., Van Wezel, R.J., Prickaerts, J.H., and van de Grind, W.A. (1993a). The dynamics of light adaptation in cat horizontal cell responses. *Vision Res.* 33, 1153–1171.
- Lankheet, M.J., Przybyszewski, A.W., and van de Grind, W.A. (1993b). The lateral spread of light adaptation in cat horizontal cell responses. *Vision Res.* 33, 1173–1184.
- Laughlin, S. (1981). A simple coding procedure enhances a neuron's information capacity. *Z Naturforsch [C]* 36, 910–912.
- Lee, B.B., Dacey, D.M., Smith, V.C., and Pokorny, J. (2003). Dynamics of sensitivity regulation in primate outer retina: The horizontal cell network. *J. Vis.* 3, 513–526.
- Lesica, N.A., and Stanley, G.B. (2004). Encoding of natural scene movies by tonic and burst spikes in the lateral geniculate nucleus. *J. Neurosci.* 24, 10731–10740.
- Lesica, N.A., Jin, J., Weng, C., Yeh, C.I., Butts, D.A., Stanley, G.B., and Alonso, J.M. (2007). Adaptation to stimulus contrast and correlations during natural visual stimulation. *Neuron* 55, 479–491.
- Lu, S.M., Guido, W., and Sherman, S.M. (1992). Effects of membrane voltage on receptive field properties of lateral geniculate neurons in the cat: Contributions of the low-threshold Ca^{2+} conductance. *J. Neurophysiol.* 68, 2185–2198.
- Machens, C.K., Wehr, M.S., and Zador, A.M. (2004). Linearity of cortical receptive fields measured with natural sounds. *J. Neurosci.* 24, 1089–1100.

- Mante, V., Frazor, R.A., Bonin, V., Geisler, W.S., and Carandini, M. (2005). Independence of luminance and contrast in natural scenes and in the early visual system. *Nat. Neurosci.* 8, 1690–1697.
- Masland, R.H. (2001). The fundamental plan of the retina. *Nat. Neurosci.* 4, 877–886.
- Meister, M., and Berry, M.J., II. (1999). The neural code of the retina. *Neuron* 22, 435–450.
- Mitra, P.P., and Pesaran, B. (1999). Analysis of dynamic brain imaging data. *Biophys. J.* 76, 691–708.
- Mukherjee, P., and Kaplan, E. (1995). Dynamics of neurons in the cat lateral geniculate nucleus: In vivo electrophysiology and computational modeling. *J. Neurophysiol.* 74, 1222–1243.
- Olshausen, B.A., and Field, D.J. (2005). How close are we to understanding v1? *Neural Comput.* 17, 1665–1699.
- Pelli, D.G. (1997). The VideoToolbox software for visual psychophysics: Transforming numbers into movies. *Spat. Vis.* 10, 437–442.
- Pillow, J.W., Paninski, L., Uzzell, V.J., Simoncelli, E.P., and Chichilnisky, E.J. (2005). Prediction and decoding of retinal ganglion cell responses with a probabilistic spiking model. *J. Neurosci.* 25, 11003–11013.
- Purpura, K., Tranchina, D., Kaplan, E., and Shapley, R.M. (1990). Light adaptation in the primate retina: Analysis of changes in gain and dynamics of monkey retinal ganglion cells. *Vis. Neurosci.* 4, 75–93.
- Ringach, D.L., Sapiro, G., and Shapley, R. (1997). A subspace reverse-correlation technique for the study of visual neurons. *Vision Res.* 37, 2455–2464.
- Rodieck, R.W., Brening, R.K., and Watanabe, M. (1993). The origin of parallel visual pathways. In *Contrast Sensitivity*, R.M. Shapley and D. Man-Kit Lam, eds. (Cambridge, MA: Bradford Books).
- Rust, N.C., and Movshon, J.A. (2005). In praise of artifice. *Nat. Neurosci.* 8, 1647–1650.
- Rust, N.C., Mante, V., Simoncelli, E.P., and Movshon, J.A. (2006). How MT cells analyze the motion of visual patterns. *Nat. Neurosci.* 9, 1421–1431.
- Sahani, M., and Linden, J.F. (2003). How linear are auditory cortical responses? In *Advances in Neural Information Processing Systems 15*, S. Becker, S. Thrun, and K. Obermayer, eds. (Cambridge, MA: MIT Press), pp. 109–116.
- Saito, H., and Fukada, Y. (1986). Gain control mechanisms in X- and Y-type retinal ganglion cells of the cat. *Vision Res.* 26, 391–408.
- Saul, A.B., and Humphrey, A.L. (1990). Spatial and temporal response properties of lagged and nonlagged cells in cat lateral geniculate nucleus. *J. Neurophysiol.* 64, 206–224.
- Schwartz, O., and Simoncelli, E.P. (2001). Natural signal statistics and sensory gain control. *Nat. Neurosci.* 4, 819–825.
- Sciar, G., Maunsell, J.H., and Lennie, P. (1990). Coding of image contrast in central visual pathways of the macaque monkey. *Vision Res.* 30, 1–10.
- Shapley, R.M., and Victor, J.D. (1978). The effect of contrast on the transfer properties of cat retinal ganglion cells. *J. Physiol.* 285, 275–298.
- Shapley, R.M., and Victor, J.D. (1979). Nonlinear spatial summation and the contrast gain control of cat retinal ganglion cells. *J. Physiol.* 290, 141–161.
- Shapley, R.M., and Victor, J.D. (1981). How the contrast gain control modifies the frequency responses of cat retinal ganglion cells. *J. Physiol.* 318, 161–179.
- Shapley, R.M., and Enroth-Cugell, C. (1984). Visual adaptation and retinal gain controls, Volume 3 (London: Pergamon).
- Sharpee, T.O., Sugihara, H., Kurgansky, A.V., Rebrik, S.P., Stryker, M.P., and Miller, K.D. (2006). Adaptive filtering enhances information transmission in visual cortex. *Nature* 439, 936–942.
- Sherman, S.M. (2001). Tonic and burst firing: Dual modes of thalamocortical relay. *Trends Neurosci.* 24, 122–126.
- Simoncelli, E.P., and Olshausen, B.A. (2001). Natural image statistics and neural representation. *Annu. Rev. Neurosci.* 24, 1193–1216.
- Smith, G.D., Cox, C.L., Sherman, S.M., and Rinzel, J. (2000). Fourier analysis of sinusoidally driven thalamocortical relay neurons and a minimal integrate-and-fire-or-burst model. *J. Neurophysiol.* 83, 588–610.
- Smyth, D., Willmore, B., Baker, G.E., Thompson, I.D., and Tolhurst, D.J. (2003). The receptive-field organization of simple cells in primary visual cortex of ferrets under natural scene stimulation. *J. Neurosci.* 23, 4746–4759.
- So, Y.T., and Shapley, R. (1981). Spatial tuning of cells in and around lateral geniculate nucleus of the cat: X and Y relay cells and perigeniculate interneurons. *J. Neurophysiol.* 45, 107–120.
- Solomon, S.G., Peirce, J.W., Dhruv, N.T., and Lennie, P. (2004). Profound contrast adaptation early in the visual pathway. *Neuron* 42, 155–162.
- Stanley, G.B., Li, F.F., and Dan, Y. (1999). Reconstruction of natural scenes from ensemble responses in the lateral geniculate nucleus. *J. Neurosci.* 19, 8036–8042.
- Troy, J.B., Bohnsack, D.L., and Diller, L.C. (1999). Spatial properties of the cat X-cell receptive field as a function of mean light level. *Vis. Neurosci.* 16, 1089–1104.
- Troy, J.B., and Shou, T. (2002). The receptive fields of cat retinal ganglion cells in physiological and pathological states: Where we are after half a century of research. *Prog. Retin. Eye Res.* 21, 263–302.
- Van Hateren, J.H. (1993). Spatiotemporal contrast sensitivity of early vision. *Vision Res.* 33, 257–267.
- van Hateren, J.H. (2007). A model of spatiotemporal signal processing by primate cones and horizontal cells. *J. Vis.* 7, 3.
- van Hateren, J.H., Ruttiger, L., Sun, H., and Lee, B.B. (2002). Processing of natural temporal stimuli by macaque retinal ganglion cells. *J. Neurosci.* 22, 9945–9960.
- Victor, J.D., and Shapley, R.M. (1979). The nonlinear pathway of Y ganglion cells in the cat retina. *J. Gen. Physiol.* 74, 671–689.
- Victor, J.D. (1987). The dynamics of the cat retinal X cell centre. *J. Physiol.* 386, 219–246.
- Victor, J.D. (1999). Temporal aspects of neural coding in the retina and lateral geniculate. *Network* 10, R1–R66.
- Wang, X., Wei, Y., Vaingankar, V., Wang, Q., Koepsell, K., Sommer, F.T., and Hirsch, J.A. (2007). Feedforward excitation and inhibition evoke dual modes of firing in the cat's visual thalamus during naturalistic viewing. *Neuron* 55, 465–478.
- Wassle, H. (2004). Parallel processing in the mammalian retina. *Nat. Rev. Neurosci.* 5, 747–757.
- Weliky, M., Fiser, J., Hunt, R.H., and Wagner, D.N. (2003). Coding of natural scenes in primary visual cortex. *Neuron* 37, 703–718.
- Yeh, T., Lee, B.B., and Kremer, J. (1996). The time course of adaptation in macaque retinal ganglion cells. *Vision Res.* 36, 913–931.